Sea level rise changes estuarine tidal stream energy

Danial Khojasteh [a, *], Shengyang Chen [a], Stefan Felder [a], William Glamore [a],

M. Reza Hashemi [b], Gregorio Iglesias [c, d]

[a] *Water Research Laboratory, School of Civil and Environmental Engineering, UNSW Sydney, NSW 2052, Australia*

[b] *Department of Ocean Engineering, Graduate School of Oceanography, The University of Rhode Island, USA*

[c] *MaREI, Environmental Research Institute & School of Engineering, University College Cork, College Road, Cork, Ireland*

[d] *University of Plymouth, School of Engineering, Marine Building, Drake Circus, Plymouth, PL4 8AA, United Kingdom*

ORCID IDs:

Danial Khojasteh: "0000-0002-6095-2885"

Shengyang Chen: "0000-0002-0141-1894"

Stefan Felder: "0000-0003-1079-6658"

William Glamore: "0000-0002-0384-8221"

M. Reza Hashemi: "0000-0002-3312-4005"

Gregorio Iglesias: " 0000-0003-2719-1663"

*** Corresponding author**
Email addresses: danial.khojasteh@unsw.edu.au; s.chen@wrl.unsw.edu.au; s.felder@unsw.edu.au; w.glamore@wrl.unsw.edu.au; reza_hashemi@uri.edu; gregorio.iglesias@ucc.ie

Abstract

Worldwide, many estuaries have the potential to harness tidal stream energy via the conversion of current velocities into a consumable energy source. However, the effects of future sea level rise on the tidal stream energy resource within different estuary types are largely unknown. To address this knowledge gap, 978 idealised hydrodynamic simulations were carried out to first identify estuary types and the location of hotspots within them that are promising for tidal energy exploitation in present-day conditions, and then provide insights into the altered tidal stream energy of different estuary types under various future sea level rise and river inflow scenarios. The results indicate that, under sea level rise, the tidal stream energy of prismatic estuaries reduces more than that of converging estuaries. This implies that estuaries that are currently worth exploiting for tidal power may cease to be in the future due to accelerating sea level rise. Further, as sea level rise may bring about geomorphic adjustments, the spatial energy patterns within an estuary may shift and optimal energy sites may be eliminated or displaced. These climate change effects pose a serious challenge for the management of tidal energy generation in future. In this context, the findings of this study are of practical significance for decision-makers in designing long-term strategies for the development of tidal energy installations in estuaries under rising mean sea levels.

Keywords: Tidal energy, tidal power, marine renewable energy, estuary, hydrodynamic modelling, climate change.

1 Introduction

The increasing energy demand due to a growing population and the contribution of fossil-fuel-related emissions to global climate change have motivated engineers and researchers to exploit carbon-friendly, predictable, and sustainable energy resources [1-7]. Among these new forms of energy, marine renewable energies can help mitigate greenhouse gas emissions and contribute to a low-carbon energy mix [8-10]. In particular, tidal stream (current) energy, which can be harnessed by tidal energy converters (e.g., turbines) using the kinetic energy of moving water, is a promising renewable energy resource due to its advantages over other renewables [11], including:

- it is more predictable than other renewable energy resources that are intermittent and involve higher operational uncertainties (e.g., wave energy) [12, 13];
- it is available in many locations worldwide (e.g., estuaries, tidal rivers, straits) [4, 14, 15];
- it has relatively well-established technology compared with other ocean renewables [16];
- it is a potential solution for less accessible areas such as islands [12];
- it holds high energy density [17, 18] and occupies less land [19]; and,
- it has reasonable investment, operation, and maintenance costs [20].

Estuaries are potentially ideal locations for tidal stream energy sites as they are located at the transition zone between rivers and open ocean, often with strong currents (due to their bathymetric and geometric characteristics), limited wave forces, and easy access to industrial and urban infrastructures [21-23]. For instance, many estuaries worldwide exhibit tidal stream velocities larger than 1 m/s, with spring tide values exceeding 2 m/s in specific locations [13]. This is important as the installation of tidal infrastructures in estuaries can help

provide the energy demand for people who live near these often densely populated areas [22], with low environmental impacts [24].

There is widespread consensus that estuaries are susceptible to climate change driven sea level rise (SLR) [25, 26] due to their low-elevation topography and proximity to the open ocean [21, 27]. The latest report from the United Nation's Intergovernmental Panel on Climate Change (IPCC) estimated that global mean sea levels will rise between 0.28 to 1.02 m by 2100, relative to the 1995–2014 average [28]. Although these are the highest projections made by the IPCC, considerable uncertainties in SLR predictions exist regarding the role of the Greenland and Antarctic ice sheets [29], and recent studies suggest the possibility of SLR exceeding 2 m by 2100 [30, 31]. While the majority of previous studies have focused on SLR impacts in estuaries in terms of changes to tidal dynamics (i.e., tidal range, current velocity, asymmetry, phase) [21, 32, 33], saline incursion [34, 35], and vegetation communities [27, 36-38], research on SLR impacts on estuarine tidal stream energy (or power) is scarce.

The tidal stream energy distribution in an estuary primarily depends on external driving forces (tides, wind, river inflows, etc.), boundary conditions (e.g., bed/bank roughness), intrinsic fluid properties (e.g., density), and estuarine geometry (e.g., shape, length, depth, bed slope) (for details, see [39]). Thus, the tidal stream energy within an estuary is site specific. To date, the spatial and temporal distributions of tidal stream energy have been investigated in various global estuaries including Ria de Ribadeo, Spain [19], Ria de Ortigueira, Spain [15], Ria de Vigo, Spain [2], Ria de Ferrol, Spain [20], Avilés, Spain [40], Minho River, at the border between Spain and Portugal [13], Severn, UK [11], Shannon, Ireland [41], Baía de Todos os Santos, Brazil [22], Chesapeake and Delaware, USA [42, 43], as well as Koksoak River, Canada [44]. These studies primarily focused on assessing the availability of tidal stream energy in local estuaries and identifying hotspots for tidal energy development. However, most of them have

disregarded the influence of SLR (except [42, 43]) on tidal current power and the location of optimal sites. Further, as these are case studies, the findings are limited to single locations and cannot be transferred from one estuary to another [21].

Accelerating SLR may influence the current velocity and thereby the available tidal energy (power), which is proportional to the current velocity cubed [42]. For instance, previous work highlights that SLR does not affect the magnitudes of maximum tidal current velocity but alters the distributions of ebb or flood velocities in idealised estuaries [21]. In addition to changes in stream velocity, SLR may impact potential hotspots for tidal stream energy development by changing the water depth, water surface area, and tidal asymmetry [42, 43, 45]. Therefore, a systematic study, which is currently absent in the literature, is useful to improve understanding of stream energy in various estuaries and develop long-term tidal energy plans, given that SLR will likely influence the operation of tidal stream energy converters and the security of energy generation – and therein lies the motivation for the present work.

To provide this information, an ensemble of estuarine hydrodynamic models was simulated to provide a systematic understanding of the tidal stream energy potential and hotspots in different estuary types under various conditions and SLR scenarios. Further, ramifications for future research and management of estuarine tidal stream energy are presented.

This paper is organised as follows. Section 2 provides an overview of the numerical method, the variables considered, and the cases simulated. Section 3 deals with the tidal stream energy potential and hotspots in mesotidal and macrotidal estuaries, and how they may be affected by SLR, in some cases to the point of becoming unviable for tidal energy harvesting. Section 4 presents a discussion on the influence of geomorphic alterations and river inflows

on the tidal stream energy resource of different estuaries. Finally, conclusions are provided in Section 5.

2 Methodology

2.1 Numerical simulations

An ensemble of estuarine hydrodynamic models comprising 978 simulations were undertaken. Three widely accepted estuarine geometries, representing many global estuaries [46-49], were considered including prismatic, weakly converging, and moderately converging. These geometries, as well as the parameters investigated and the coordinate system, are illustrated in Fig. 1. While a prismatic estuary has a constant width (Fig. 1(a)), the width of converging estuaries is a function of the distance from the mouth, $B(x) = B_0 \exp(-x/L_c)$, where x is the distance from the mouth, B_0 denotes the width at the mouth, and L_c is the width convergence length [48]. Here, L_c = 160 km and L_c = 80 km (Fig. (b, c)) were considered to represent typical weakly and moderately converging estuaries.

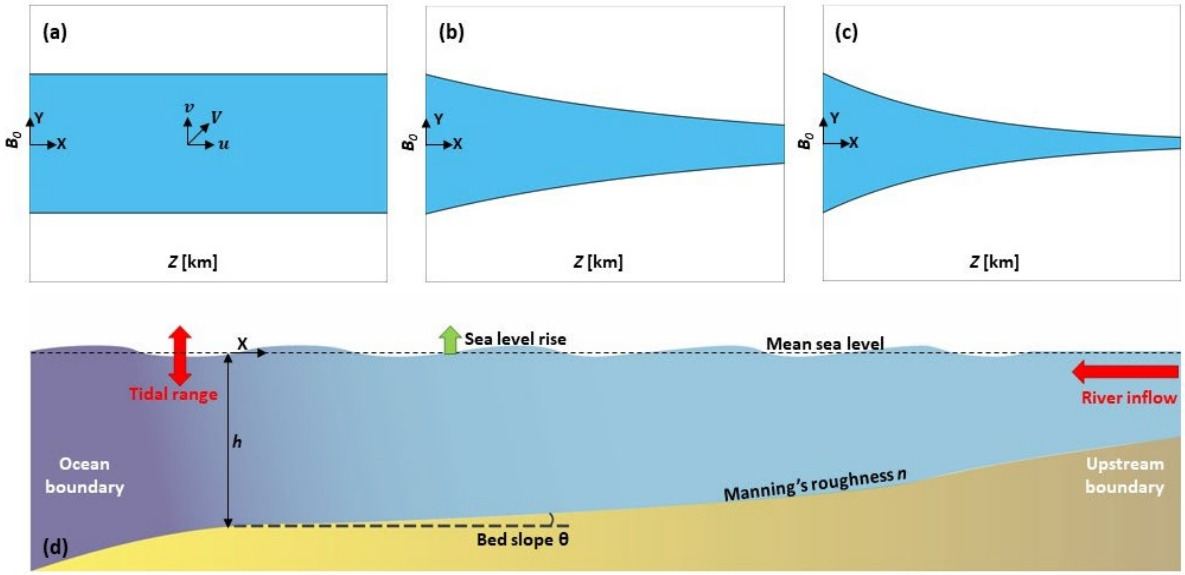

Fig. 1. Schematic of estuary types considered in this study: top view of (a) prismatic, (b) converging with L_c = 160 km; and (c) converging with L_c = 80 km estuaries, and side view (d) with boundary conditions including tides and river inflow as driving forces.

To ensure that the results of this study have the potential to be transferred back to real-world estuaries, a range of parameters in line with existing estuaries were varied across the simulations. These parameters are presented in Table 1, and include estuary length (Z), tidal range at the mouth (TR_0), Manning's roughness (n), river inflow over tidal prism (Q/TP) ratios, and SLR scenarios. Three lengths were considered to highlight the importance of estuary length on tidal stream energy comprising Z = 40, 80, and 160 km [32], representing short, moderate, and long estuaries, respectively. Two distinct tidal ranges at the entrance were applied to represent mesotidal (TR_0 = 1 m) and macrotidal (TR_0 = 4 m) estuaries [50]. Tides at the entrance were assumed to be the main semidiurnal tidal constituent M2 with a perfect sinusoidal signal and a period (T) of 12.42 hours. Three different SLR scenarios were considered including SLR = 0 m (base case), SLR = 1 m, and SLR = 2 m. To examine the significance of roughness of bed/banks, three values of Manning's n were applied including n = 0.015, 0.03, and 0.09 s/m$^{1/3}$ [51], representing low, moderate, and high friction scenarios, respectively. For all base cases (cases with SLR = 0 m), the tidal prism (the volume of water that enters an estuary over a tidal cycle) was measured, and a constant river inflow (Q) with a desired percentage of the tidal prism was applied at the head of the estuaries that have upstream river inflow. The values of this inflow were within the range of real sites presented in [52], representing the altered precipitation pattern under climate change and seasonal or geographical variability of estuarine tidal stream power during zero (Q/TP = 0%), low (Q/TP = 1%), medium (Q/TP = 5%), and high (Q/TP = 10%) river inflow conditions.

The changes in the variables presented in Table 1 resulted in 972 runs comprising 324 prismatic cases (162 cases for TR_0 = 1 m, and 162 cases for TR_0 = 4 m), 324 converging cases with L_c = 160 km (162 cases for TR_0 = 1 m, and 162 cases for TR_0 = 4 m), and 324 converging cases with L_c = 80 km (162 cases for TR_0 = 1 m, and 162 cases for TR_0 = 4 m). For instance, out

of 162 cases for prismatic estuaries with TR_0 = 1 m, 54 runs are base cases (SLR = 0 m), 54 runs are for SLR = 1 m scenario, and 54 runs are for SLR = 2 m scenario. Further, two bed conditions were modelled including a flat (θ = 0°) and sloped bed (θ = 0.004°, applied so that the water depth reduces linearly from its initial value at the mouth to zero at the head of the base case) to better represent real-world estuaries [53]. The influence of bed slope is only discussed in the Section 4, where six more simulation cases were carried out, and hence, bed slope is not presented in Table 1.

For simplicity, other driving forces of the estuarine circulation (wind, barotropic or baroclinic effects) and real time geomorphic variations were not considered. The effect of Coriolis force was ignored as it was found that it only altered the outcomes (i.e., stream velocity and power) of examined cases by less than 0.1%, thus providing latitude-independent research. All estuaries considered were assumed to be protected by levees and dykes to prevent adjacent lands from overbank inundation. As only M2 tides were considered, the findings of the present study may only be applicable to semi-diurnal estuaries. Further, as other tidal constituents were not considered, the nonlinear interaction between all constituents that may generate tidal asymmetry [54] was disregarded. All estuaries were assumed to be well-mixed and hence, the influence of stratification was not considered. As such, the findings of the present study may provide an initial guideline on the available tidal energy resource and hotspots within different estuary types as well as how they may be influenced by SLR. If a real-world estuary matches one of the cases examined here with potential for harnessing tidal stream energy, an advanced hydrodynamic modelling of the system is recommended to gain detailed insights into the tidal energy potential, location of top sites, and how they may be altered under SLR.

Table 1. Variables and their corresponding values considered in the simulations of prismatic, converging with L_c = 80 km, and converging with L_c = 80 km estuaries.

Variable	Value
Estuary length (Z) [km]	40, 80, 160
Estuary width (B) [m]	1000
Estuary depth (h) [m]	5
Water density (ρ) [kg/m^3]	1020
Tidal range at the mouth (TR_0) [m]	1, 4
Sea level rise (SLR) [m]	0, 1, 2
River inflow/Tidal prism (Q/TP) [%]	0, 1, 5, 10
Tidal period (T) [hour]	12.42
Manning's coefficient (n) [s/m$^{1/3}$]	0.015, 0.03, 0.09

2.2 Tidal stream energy estimation

The magnitude of the depth-averaged (over water depth along the centreline of each case) and time-averaged (e.g., over a full spring-neap tidal cycle, ~15 days) mean total velocity V in terms of the horizontal velocity components (Fig. 1(a)) is determined as follows:

$$V = \sqrt{u^2 + v^2} \tag{1}$$

where u is the longitudinal (X-axis) mean stream velocity component and v is the lateral (Y-axis) mean stream velocity component (Fig. 1), both depth- and time-averaged along the centreline of each case. The instantaneous mean tidal stream power density, i.e., mean tidal stream power per unit cross-sectional area perpendicular to the flow direction, P [W/m^2], is calculated as [55, 56]:

$$P = \frac{1}{2}\rho V^3 \tag{2}$$

where ρ denotes the density of water. Also, using the time integral, the averaged power density $\bar{P}$ [W/m^2] over a certain period t (here, over a full spring-neap tidal cycle, $t \simeq 15$ days) can be estimated as follows [42]:

$$\bar{P} = \frac{1}{t}\int_0^t \frac{1}{2}\rho V^3 dt \tag{3}$$

2.3 Model description

In this study, the RMA-2 hydrodynamic modelling package [57] was used to solve the depth-averaged form of the Reynolds-averaged Navier-Stokes equations (known as the shallow water equations) to identify the flow field, water surface elevations, and horizontal velocity components in an estuarine system [58, 59]. To this end, it utilises the Galerkin finite element method and adopts horizontal eddy viscosity coefficients to define turbulence characteristics of each element. As it uses a Crank Nicholson implicit time integration scheme during transient conditions, the stability of each run is independent of the Courant condition [21, 57].

Several grid-independence tests were conducted to determine the optimum mesh resolution (MR) for the numerical simulations. To this end, five MRs of 50, 100, 250, 500, and 1000 m were examined, and plots of V and P for a prismatic macrotidal estuary with Z = 40 km, Q/TP = 10%, and n = 0.015 s/m$^{1/3}$ are presented in Fig. 2. The percentage changes of calculated V and P for MRs of 100, 250, 500, and 1000 m compared to a MR of 50 m are 0-0.5% and 0-1.6%; 0-3% and 0-9%; 0-4% and 0-11%; and 0-9% and 0-25%, respectively. As such, a MR of 100 m was selected to discretise the estuaries with quadrilateral elements. Each simulation case was run for a period of 30 days with a time step of 15 minutes. The results of the first 10 days were then discarded to avoid the instabilities of the initialisation process. The flow field, water surface elevations, and horizontal velocity components were then processed for the remaining period. Further information regarding the RMA-2 modelling suite and the accuracy of the model (model validation for the idealised framework) is available in previous works [21, 58].

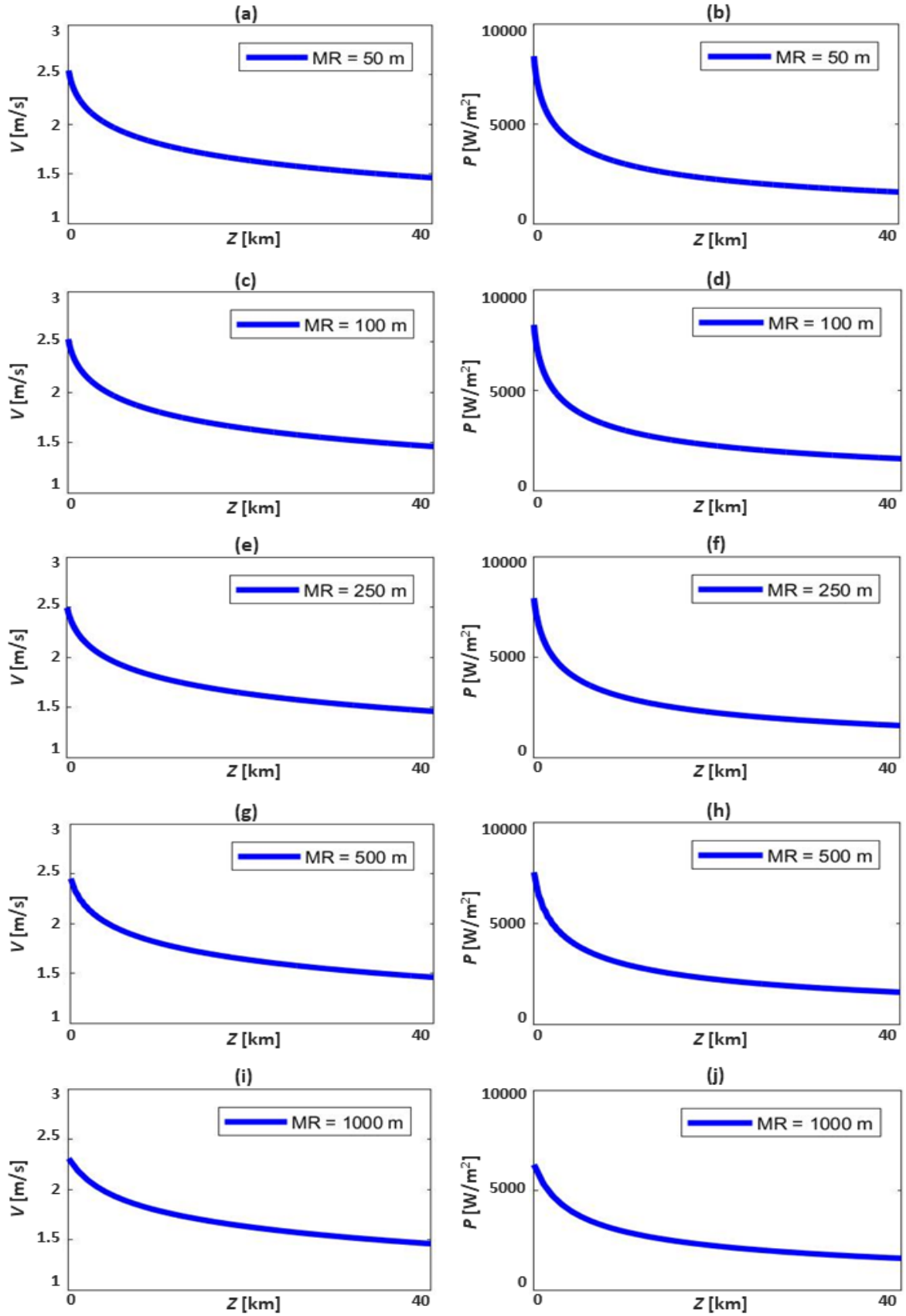

Fig. 2. Grid-independence study for a prismatic macrotidal (TR_0 = 4 m) estuary where Z = 40 km, Q/TP = 10%, and n = 0.015 s/m$^{1/3}$ with mesh resolutions (MR) of (a, b) 50 m, (c, d) 100 m, (e, f) 250 m, (g, h) 500 m, and (i, j) 1000 m.

3 Results

All cases were filtered to identify estuaries that contain areas with $V \geq 1$ m/s or $P \geq 510$ W/m^2. These thresholds generally ensure that the sites are worth exploiting and most 3rd generation tidal stream energy converters are functional, as they can be used in all water depths and generate relatively constant electricity [60]. Table 2 presents the mesotidal and macrotidal estuaries with different boundary conditions and certain areas (lengths) with $P \geq$ 510 W/m^2, which are suitable to harvest tidal stream energy in present-day conditions. Further, this table shows the influence of SLR (1 and 2 m of SLR as near future and far future scenarios, respectively) on the location of optimal sites and the amount of tidal stream power for different cases. This filtration analysis can provide a better understanding about the estuaries that are currently viable for tidal stream energy extraction and the potential impacts of SLR on the spatial distribution of stream velocity, energy, and hotspots for tidal infrastructure development, as well as managing tidal energy generation in the future. For estuaries with $P \geq 510$ W/m^2 (or $V \geq 1$ m/s), P, $\bar{P}$, and V were calculated and typical results are presented in the following sections. The feasible estuaries for exploiting tidal stream energy in present-day conditions (SLR = 0 m) are discussed in Section 3.1, and the influence of SLR on tidal power and energy hotspots of these estuaries is described in Section 3.2. In all figures below, blue, red, and green curves indicate SLR = 0, 1, and 2 m, respectively. Where appropriate, two dashed lines of V = 1 m/s and P = 510 W/m^2 are added to the plots to better indicate the location of optimal sites and their potential displacement or disappearance under SLR.

Table 2. Mesotidal and macrotidal estuaries of different shapes with areas of $V \geq 1$ m/s in present-day (SLR = 0 m) conditions for tidal development and the influence of 1 and 2 m of SLR on these estuaries (for all cases here, θ = 0°).

Estuary type	**Estuary shape**	***Q/TP* (%)**	***Z* [km]**	***n* [s/m$^{1/3}$]**	**Energy hotspot length [km] when SLR = 0 m and corresponding *P* [W/m^2]**	**Energy hotspot length [km] under SLR = 1 m and corresponding *P* [W/m^2]**	**Energy hotspot length [km] under SLR = 2 m and corresponding *P* [W/m^2]**
Mesotidal (TR_0 = 1 m)	Converging with L_c = 160 km	10	160	0.015	113-160 km (510-844 W/m^2)	130-160 km (510-740 W/m^2)	146-160 km (510-616 W/m^2)
	Converging with L_c = 80 km	5	160	0.015	108-160 km (510-1956 W/m^2)	118-160 km (510-1696 W/m^2)	127-160 km (510-1399 W/m^2)
		10	40	0.015	31-40 km (510-640 W/m^2)	Infeasible	Infeasible
			80	0.015	42-80 km (510-1309 W/m^2)	54-80 km (510-1069 W/m^2)	64-80 km (510-832 W/m^2)
				0.03	73-80 km (510-585 W/m^2)	Infeasible	Infeasible
			160	0.015	48-160 km (510-6777 W/m^2)	59-160 km (510-6520 W/m^2)	69-160 km (510-6114 W/m^2)
				0.03	79-160 km (510-2603 W/m^2)	82-160 km (510-2577 W/m^2)	87-160 km (510-2532 W/m^2)
Macrotidal (TR_0 = 4 m)	Prismatic	5	40	0.015	0-14 km (1370-510 W/m^2)	0-5 km (890-510 W/m^2)	Infeasible
				0.03	0-5 km (1068-510 W/m^2)	0-1 km (631-510 W/m^2)	Infeasible
				0.09	0-1 km (746-510 W/m^2)	Infeasible	Infeasible
			80	0.015	0-4 km (953-510 W/m^2)	0-1 km (633-510 W/m^2)	Infeasible
				0.03	0-1 km (651-510 W/m^2)	Infeasible	Infeasible
			160	0.015	0-6 km (936-510 W/m^2)	0-1 km (550-510 W/m^2)	Infeasible
				0.03	0-1 km (665-510 W/m^2)	Infeasible	Infeasible
		10	40	0.015	0-40 km (7647-1593 W/m^2)	0-40 km (4466-1390 W/m^2)	0-40 km (2730-1176 W/m^2)
				0.03	0-40 km (6361-720 W/m^2)	0-40 km (3956-685 W/m^2)	0-40 (2535-636 W/m^2)
				0.09	0-8 km (4274-510 W/m^2)	0-2 km (2925-510 W/m^2)	0-1 km (2032-510 W/m^2)
			80	0.015	0-80 km (4538-658 W/m^2)	0-80 km (1943-587 W/m^2)	0-75 km (1783-510 W/m^2)
				0.03	0-40 km (3837-510 W/m^2)	0-35 km (2326-510 W/m^2)	0-27 km (1486-510 W/m^2)
				0.09	0-5 km (2656-510 W/m^2)	0-4 km (1763-510 W/m^2)	0-3 km (1198-510 W/m^2)
			160	0.015	0-160 km (4781-518 W/m^2)	0-141 km (2811-510 W/m^2)	0-75 km (1700-510 W/m^2)
				0.03	0-41 km (3943-510 W/m^2)	0-37 km (2389-510 W/m^2)	0-29 km (1521-510 W/m^2)
				0.09	0-5 km (2727-510 W/m^2)	0-4 km (1813-510 W/m^2)	0-3 km (1234-510 W/m^2)

	Converging with L_c = 160 km	5	40	0.015	0-40 km (1135-542 W/m^2)	0-3 km (687-510 W/m^2)	Infeasible
				0.03	0-5 km (995-510 W/m^2)	0-1 km (556-510 W/m^2)	Infeasible
				0.09	0-1 km (773-510 W/m^2)	Infeasible	Infeasible
			80	0.015	0-5 & 74-80 km (926-510 & 510-550 W/m^2)	0-1 km (597-510 W/m^2)	Infeasible
				0.03	0-1 km (600-510 W/m^2)	Infeasible	Infeasible
			160	0.015	0-4 & 78-160 km (798-510 & 510-1205 W/m^2)	96-160 km (510-1083 W/m^2)	114-160 km (510-940 W/m^2)
				0.03	0-1 & 143-160 km (616-510 & 510-597 W/m^2)	147-160 km (510-577 W/m^2)	154-160 km (510-546 W/m^2)
		10	40	0.015	0-40 km (6994-2242 W/m^2)	0-40 km (3884-2038 W/m^2)	0-40 km (2355-1794 W/m^2)
				0.03	0-40 km (6469-1202 W/m^2)	0-40 km (3687-1153 W/m^2)	0-40 km (2272-1082 W/m^2)
				0.09	0-8 km (4773-510 W/m^2)	0-7 km (3119-510 W/m^2)	0-6 km (2034-510 W/m^2)
			80	0.015	0-80 km (4380-2389 W/m^2)	0-80 km (2541-2169 W/m^2)	0-80 km (1620-1889 W/m^2)
				0.03	0-80 km (3681-995 W/m^2)	0-80 km (2158-970 W/m^2)	0-80 km (1354-931 W/m^2)
				0.09	0-5 km (2434-510 W/m^2)	0-4 km (1679-510 W/m^2)	0-3 km (1137-510 W/m^2)
			160	0.015	0-160 km (4322-4086 W/m^2)	0-160 km (2549-4695 W/m^2)	0-160 km (1550-3847 W/m^2)
				0.03	0-160 km (3789-1879 W/m^2)	0-160 km (2221-1866 W/m^2)	0-160 km (1391-1845 W/m^2)
				0.09	0-5 km (2499-510 W/m^2)	0-4 km (1728-510 W/m^2)	0-3 km (1173-510 W/m^2)
	Converging with L_c = 80 km	5	40	0.015	0-40 km (919-922 W/m^2)	22-40 km (510-757 W/m^2)	35-40 km (510-575 W/m^2)
				0.03	1-4 & 34-40 km (833-510 & 510-561 W/m^2)	Infeasible	Infeasible
				0.09	0-1 km (662-510 W/m^2)	Infeasible	Infeasible
			80	0.015	0-5 & 23-80 km (757-510 & 510-1824 W/m^2)	39-80 km (510-1513 W/m^2)	50-80 km (510-1227 W/m^2)
				0.03	52-80 km (510-866 W/m^2)	58-80 km (510-811 W/m^2)	65-80 km (510-734 W/m^2)
			160	0.015	0-6 & 19-160 km (737-510 & 510-11338 W/m^2)	38-160 km (510-9275 W/m^2)	49-160 km (510-8829 W/m^2)
				0.03	51-160 km (510-4368 W/m^2)	58-160 km (510-4331 W/m^2)	63-160 km (510-4270 W/m^2)
				0.09	128-160 km (510-950 W/m^2)	129-160 km (510-948 W/m^2)	130-160 km (510-947 W/m^2)
		10	40	0.015	0-40 km (5894-3688 W/m^2)	0-40 km (3245-3393 W/m^2)	0-40 km (1961-3026 W/m^2)

				0.03	0-40 km (5505-1940 W/m^2)	0-40 km (3109-1872 W/m^2)	0-40 km (1907-1772 W/m^2)
				0.09	0-9 km (4141-510 W/m^2)	0-8 km (2671-510 W/m^2)	0-7 km (1730-510 W/m^2)
			80	0.015	0-80 km (3900-7100 W/m^2)	0-80 km (2212-6698 W/m^2)	0-80 km (1374-6135 W/m^2)
				0.03	0-80 km (3350-2809 W/m^2)	0-80 km (1948-2768 W/m^2)	0-80 km (1214-2703 W/m^2)
				0.09	0-5 & 69-80 km (2249-510 & 510-618 W/m^2)	0-4 & 70-80 km (1539-510 & 510-617 W/m^2)	0-3 & 70-80 km (1037-510 & 510-615 W/m^2)
			160	0.015	0-160 km (3997-36761 W/m^2)	0-160 km (2204-30465 W/m^2)	0-160 km (1351-27837 W/m^2)
				0.03	0-160 km (3454-13580 W/m^2)	0-160 km (2008-13558 W/m^2)	0-160 km (1251-13521 W/m^2)
				0.09	0-5 & 68-160 km (2312-510 & 510-2916 W/m^2)	0-4 & 68-160 km (1587-510 & 510-2916 W/m^2)	0-3 & 69-160 km (1070-510 & 510-2914 W/m^2)

3.1 Tidal stream velocity and power in present-day conditions (without sea level rise)

The focus of this section is on the spatial distribution of tidal stream velocity, energy, and hotspots of mesotidal and macrotidal estuaries in present-day conditions (SLR = 0 m). Table 2 highlights that in mesotidal estuaries, there are no prismatic cases (out of 54 runs) with a location within the estuary with $V \geq 1$ m/s (or $P \geq 510$ W/m^2), hence limiting the application of tidal energy exploitation. Only 1 converging case with L_c = 160 km (out of 54 runs), and 6 converging cases with L_c = 80 km (out of 54 runs) exhibit potential areas ($V \geq 1$ m/s or $P \geq 510$ W/m^2) for tidal stream energy development. From Table 2, it is evident that the upstream reaches of these 7 estuaries with medium and large inflows are promising for developing tidal energy infrastructures as the energy of the currents is funnelled into smaller cross-sections and/or is strengthened by the upstream river inflows, so that the maximum tidal stream velocity and power occur at the head. Further, increasing estuary length or decreasing Manning's *n* would generally increase the tidal stream power and energy hotspot length (a length over which $V \geq 1$ m/s or $P \geq 510$ W/m^2). For instance, Fig. 3 shows the plots of V and P for a mesotidal converging estuary with L_c = 80 km with Q/TP = 10%, Z = 160 km, and n =

0.03 s/m$^{1/3}$. It is apparent that 51% of the upstream area (from 79 to 160 km) has locations with $1 \leq V \leq 1.72$ m/s corresponding to $510 \leq P \leq 2603$ W/m^2.

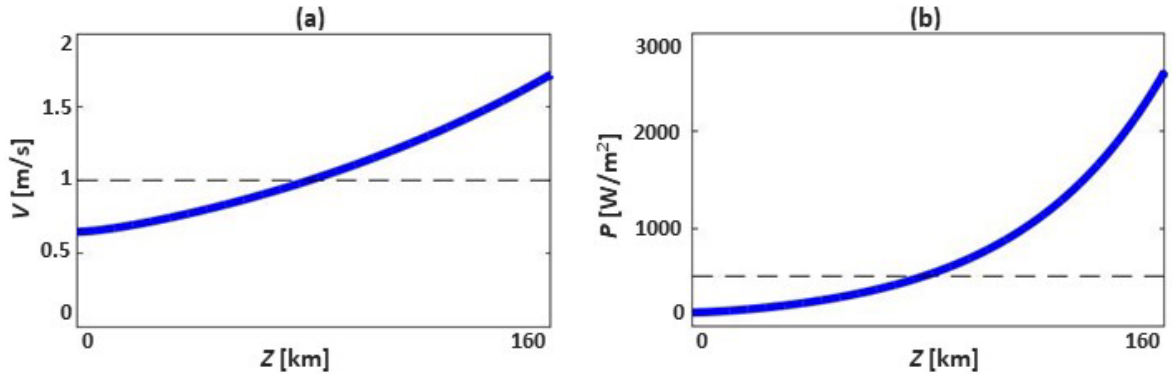

Fig. 3. Stream velocity (a) and power (b) for a converging with L_c = 80 km mesotidal (TR_0 = 1 m) estuary where Z = 160 km, Q/TP = 10%, and n = 0.03 s/m$^{1/3}$. Dashed lines show the applied feasibility thresholds for $V \geq 1$ m/s and $P \geq 510$ W/m^2.

In macrotidal estuaries in Table 2, there are 16 prismatic cases (out of 54 runs) which have areas with $V \geq 1$ m/s or $P \geq 510$ W/m^2. In these estuaries, stream velocity and power decrease by increasing length due to frictional effects and head loss in the system [21]. Further, the estuary mouth presents the highest current velocity and power in these cases. The shortest prismatic estuary has a higher percentage of suitable length for tidal energy development in comparison to moderate and long prismatic estuaries. For instance, for a prismatic estuary with Q/TP = 10% and n = 0.03 s/m$^{1/3}$, 100% of the length of a short estuary is suitable for tidal energy extraction. This ideal length reduces to the first 50% and 26% for moderate and long estuaries, respectively.

There are 16 (out of 54 runs) converging estuaries with L_c = 160 km and 17 (out of 54 runs) converging estuaries with L_c = 80 km with areas of $V \geq 1$ m/s or $P \geq 510$ W/m^2. The stream velocity and power of short converging estuaries are similar to prismatic ones where the mouth and head have the maximum and minimum values, respectively. For moderate and

long converging estuaries, the energy of the moving water is funnelled into smaller cross-sections due to the convergence of the banks, and is transmitted seaward due to the presence of protective (and reflective) walls in the upper estuary [61], as in the Bristol Channel and Severn estuary [62]. This is the main reason that stream velocity and power increase from the mouth towards the head of these systems.

Among the macrotidal estuaries, if the estuary is short, prismatic cases present largest tidal stream velocity and power but the rate of energy loss from the mouth towards the head is significant. Among moderate and long macrotidal estuaries, converging cases with L_c = 80 km generally contain the highest values of stream velocity and power, as illustrated in Fig. 4. As is clear from Fig. 4, V and P curves for a prismatic estuary reduce exponentially from the mouth towards the head, and only the first 4 km is worth considering for tidal energy instalments (Fig. 4(a, b)). For a converging estuary with L_c = 160 km, there is a fall and rise in V and P curves, with the first 5 km and the last 6 km as energy hotspots (Fig. 4(c, d)). A converging estuary with L_c = 80 km exhibits the highest values of V and P, with the first 5 km and the last 57 km as the ideal area for the installations of tidal energy devices. These findings are in line with the definitions of hyposynchronous and hypersynchronous conditions, where an estuary can experience a tidal energy amplification due to channel convergence (e.g., in converging estuaries with L_c = 80 km) or dampening due to frictional effects (e.g., in prismatic estuaries) in landward direction, respectively [63, 64].

The findings in this section can help researchers better identify estuaries with potentials for tidal energy development. Where a real-world estuary matches one of these idealised cases, a detailed hydrodynamic modelling of the site is recommended to accurately assess the tidal energy resource and determine the location of energy hotspots.

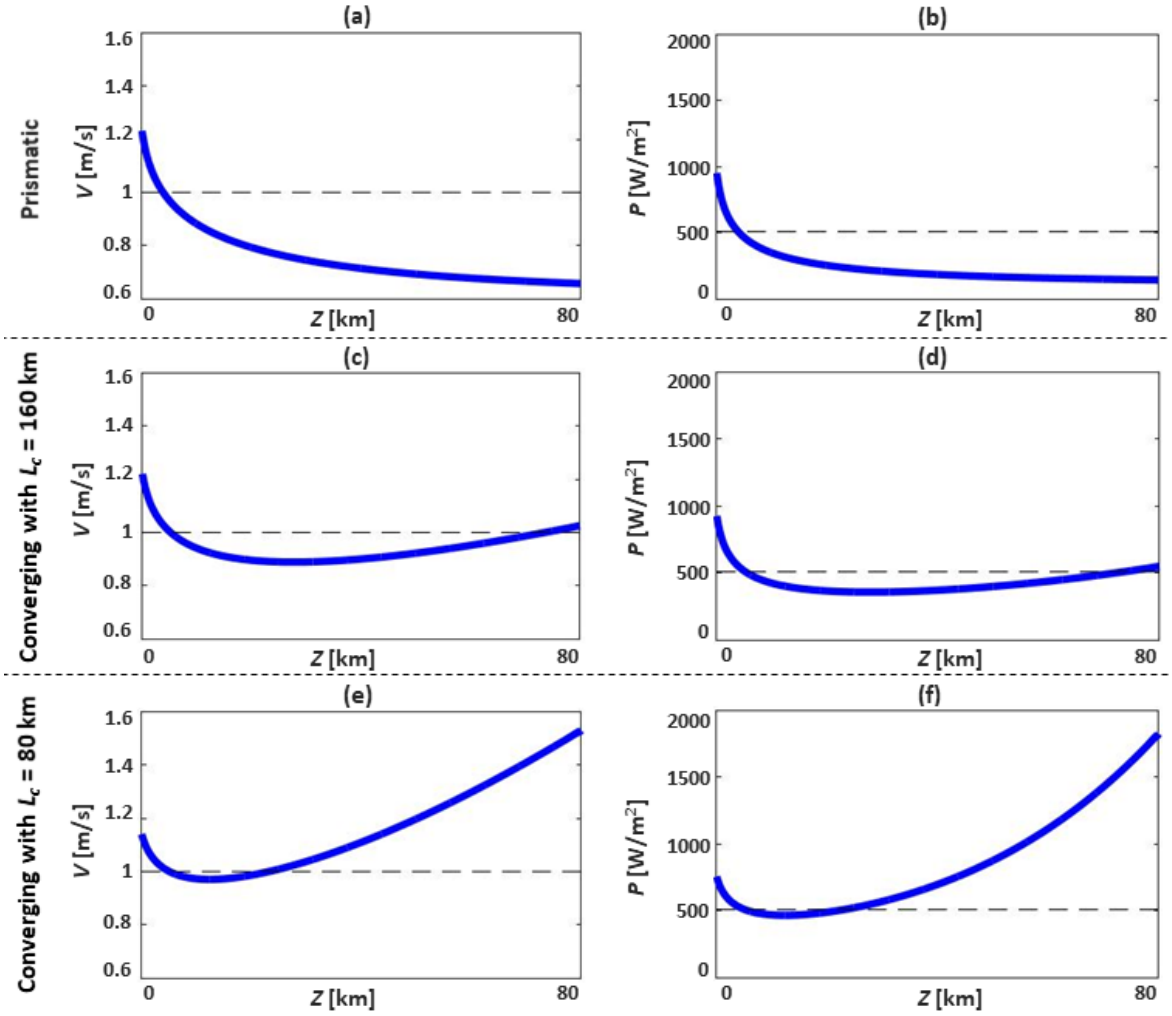

Fig. 4. Stream velocity (a, c, e) and power (b, d, f) for prismatic, converging with L_c = 160 km, and converging with L_c = 80 km macrotidal (TR_0 = 4 m) estuaries where Z = 80 km, Q/TP = 5%, and n = 0.015 s/m$^{1/3}$. Dashed lines show the applied feasibility thresholds for $V \geq 1$ m/s and $P \geq 510$ W/m^2.

3.2 Tidal stream velocity and power under sea level rise

It can be inferred from Table 2 that some of the estuaries that are currently worth exploiting for tidal power (see Section 3.1) may cease to be in the future under SLR. In mesotidal estuaries, areas of $V \geq 1$ m/s or $P \geq 510$ W/m^2 are eliminated under 1 and 2 m of SLR for two converging estuaries with L_c = 80 km, which is indicated as "Infeasible" in Table 2, leaving only 5 cases (out of 54 runs for each SLR scenario) with the potential to harvest tidal current energy.

Further, the influence of SLR on short estuaries is more evident in comparison to longer ones. For instance, a converging mesotidal estuary with L_c = 80 km, Q/TP = 10%, Z = 40 km, and n = 0.015 s/m$^{1/3}$ meets the criterion ($V \geq 1$ m/s or $P \geq 510$ W/m^2) to extract tidal stream energy at certain locations when SLR = 0 m (present-day conditions) but does not have any locations or zones with $V \geq 1$ m/s or $P \geq 510$ W/m^2 under SLR = 1 and 2 m (Fig. 5(a, b) and Table 2). However, the tidal stream velocity and power of a similar estuary with Z = 160 km decrease minimally under SLR (Fig. 5(e, f)). The changes in current velocity under SLR are consistent with [21], where it has been reported that SLR marginally decreases the tidal current velocity along the centre line of long estuaries. Further, it has been analytically demonstrated that the stream velocity is slightly reduced with increasing water depth, which mimics future SLR [49]. SLR also diminishes the areas of interest for tidal energy infrastructures. To illustrate, when Z = 80 km (Fig. 5(c, d)), the base case (no SLR) has areas of $V \geq 1$ m/s or $P \geq 510$ W/m^2 in 47% of the upstream length. SLR of 1 and 2 m reduces this length to 32% and 20%, respectively. Variations in the distribution of tidal stream velocity and power under SLR would change the locations of hotspots for energy extraction, which should be considered in future management and development of tidal infrastructures. This finding is highlighted in [42] where a shift in the distribution of optimum sites for tidal energy installations along the New Jersey coastlines was observed under 1 m of SLR.

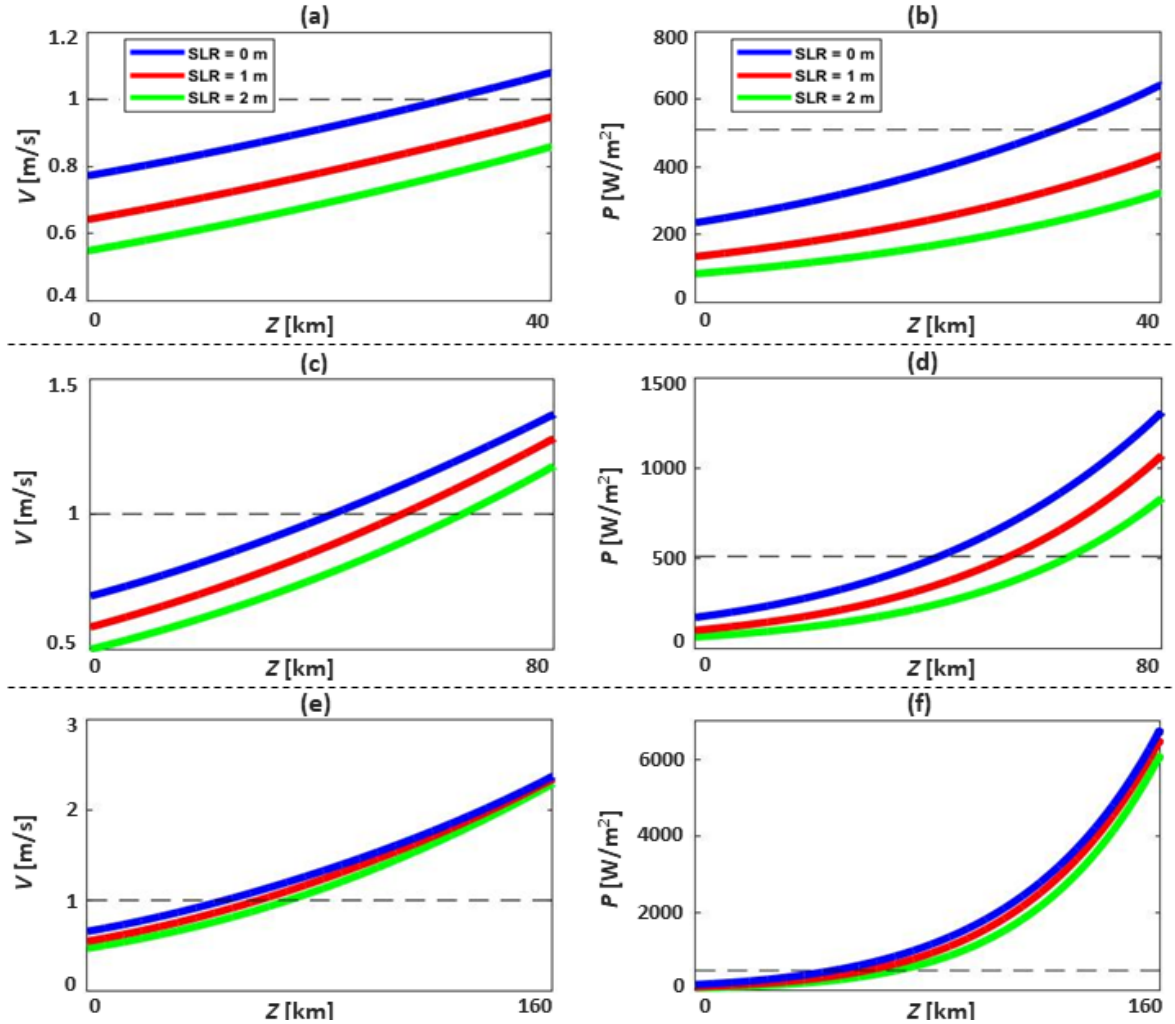

Fig. 5. Stream velocity (a, c, e) and power (b, d, f) for converging with L_c = 80 km mesotidal (TR_0 = 4 m) estuaries where Z = 40, 80, and 160 km, Q/TP = 10%, and n = 0.015 s/m$^{1/3}$. Dashed lines show the applied feasibility thresholds for $V \geq 1$ m/s and $P \geq 510$ W/m^2.

According to Section 3.1 for macrotidal estuaries, there were 16, 16, and 17 prismatic, converging with L_c = 160 km, and converging with L_c = 80 km estuaries, respectively, with areas of $V \geq 1$ m/s or $P \geq 510$ W/m^2 in present-day conditions. SLR of 1 m will eliminate 3 prismatic, 2 converging with L_c = 160 km, and 2 converging with L_c = 80 km base cases, while SLR of 2 m will eliminate 7, 5, and 2 base cases, respectively. In prismatic estuaries, all cases with Q/TP = 5% will become unviable under 2 m of SLR. In converging estuaries with L_c = 160 km, short and moderate estuaries with Q/TP = 5% will become infeasible under 2 m of SLR. In converging

estuaries with L_c = 80 km, SLR of 1 and 2 m will only eliminate areas of $V \geq 1$ m/s or $P \geq 510$ W/m^2 in short estuaries.

To highlight a typical result, Fig. 6 depicts the plots of V and P for different macrotidal estuaries when Q/TP = 5%, Z = 160 km, and n = 0.03 s/m$^{1/3}$. SLR reduces the speed and power of estuarine currents. This reduction is more evident in prismatic and converging estuaries with L_c = 160 km, though converging estuaries with L_c = 80 km are least influenced and the most promising systems for exploitation of tidal stream energy in present-day and future conditions. When moving from the mouth towards the head, current velocity and power decrease along a prismatic estuary (Fig. 6(a, b)) due to energy loss caused by frictional effects [21], decrease and then increase in a converging estuary with L_c = 160 km (Fig. 6(c, d)), and increase in a converging estuary with L_c = 80 km due to energy convergence [61, 65]. This is in line with analytical studies indicating that tidal energy can be amplified if $L_c \ll 3\pi h\omega/8C_D U\mathrm{K}$, where ω is tidal frequency, C_D is the drag coefficient ($C_D = gn^2h^{-1/3}$), U is the tidal current velocity amplitude, and K is the wave number [65, 66]. Thus, estuaries with a smaller magnitude of L_c (i.e., stronger convergence) would have a higher chance of tidal energy amplification in landward direction.

Further, sites for tidal energy extraction may be either unfavourably affected or benefit from SLR [42, 43]. To illustrate, a converging estuary with L_c = 160 km (Fig. 6(c, d)) has its maximum stream velocity/power at both its mouth and head, but under a SLR of 1 or 2 m, the location of the maximum values shifts to the upstream reaches. This variation, in turn, can potentially eliminate some of the existing sites near the mouth and create new hotspots further upstream. In the Mid-Atlantic-Bight, SLR would cause a few hotspots to disappear along the New Jersey coastlines facing the Atlantic Ocean but bring about new sites in the Delaware estuary, which is located in the same region [42, 43]. Therefore, accelerating SLR has

substantial implications for tidal energy management over the coming years, underscoring a need to identify future risks and develop holistic and long-term management strategies.

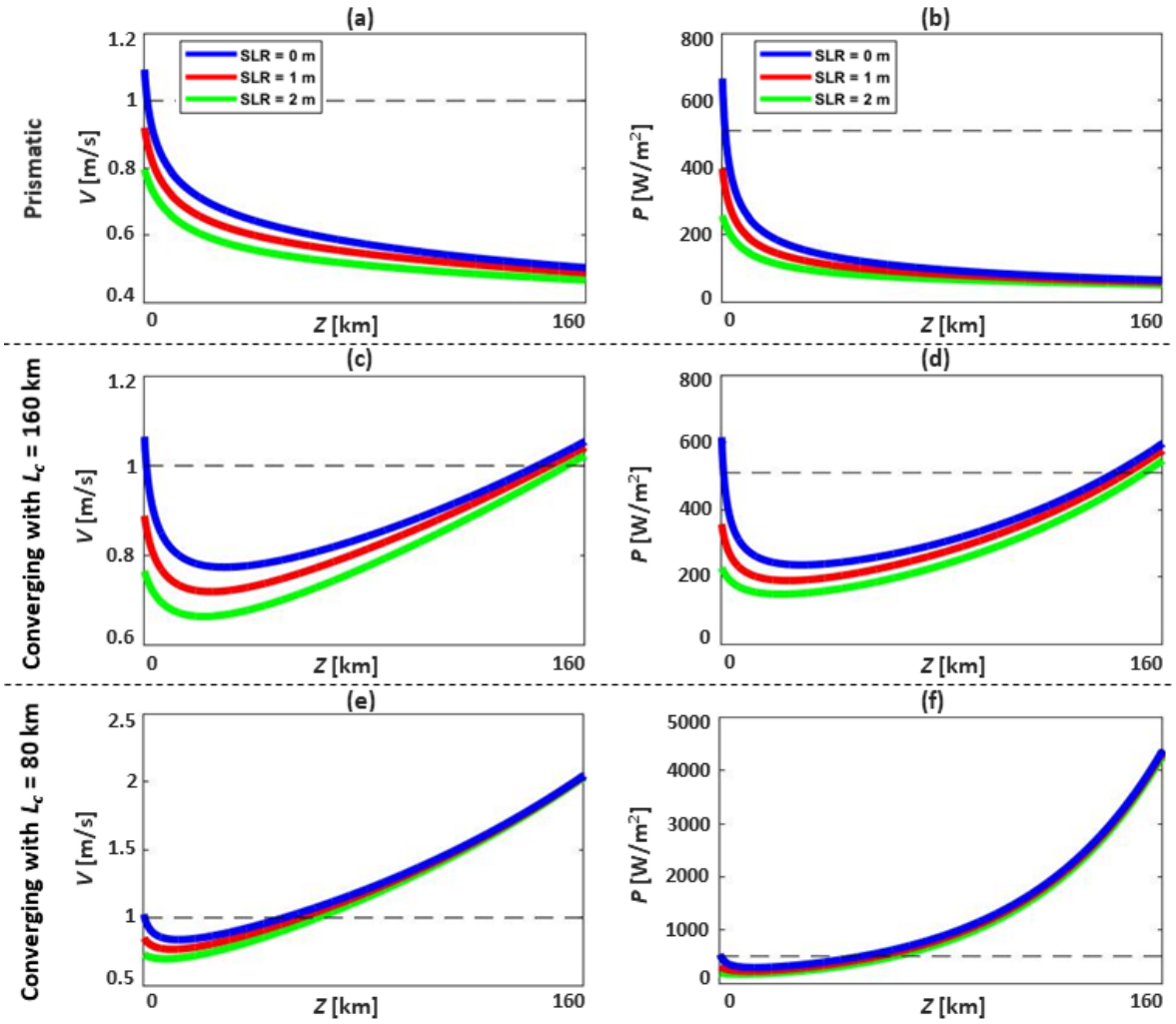

Fig. 6. Stream velocity (a, c, e) and power (b, d, f) for prismatic, converging with L_c = 160 km, and converging with L_c = 80 km macrotidal (TR_0 = 4 m) estuaries where Z = 160 km, Q/TP = 5%, and n = 0.03 s/m$^{1/3}$. Dashed lines show the applied feasibility thresholds for $V \geq 1$ m/s and $P \geq 510$ W/m^2.

4 Discussion

4.1 Estuarine geomorphology and tidal stream power

As indicated in Section 3, SLR can alter stream velocity and thereby the available stream power in an estuarine system. In a real estuary, any variations in current velocity (e.g., induced by SLR) can bring about changes to sediment erosion, suspension, and deposition – the

processes that primarily govern the geomorphology of an estuarine system [67]. Any potential adjustments in estuarine geomorphology under SRL can result in further changes in the stream velocity [68] and power. Thus, there is an ongoing feedback loop between the current velocity (and power) and the geomorphology of the system. To highlight the importance of geomorphic changes, Fig. 7 shows the spatial distribution of $\bar{P}$ for selected prismatic, converging with L_c = 160 km, and converging with L_c = 80 km macrotidal estuaries when Z = 80 km, Q/TP = 5%, and n = 0.03 s/m$^{1/3}$, representing typical results of tested cases. It is noticeable that converging estuaries (Fig. 7(b, c)) retain larger stream power in comparison to prismatic estuaries. Therefore, if over time, the shape of an estuary (or part of it) shifts from prismatic to converging, or vice versa (e.g., under SLR), there will be a variation in its potential for the exploitation of tidal stream power.

Another potential geomorphic alteration in estuaries is the changing bed form under SLR and/or due to energy extraction. As mentioned above, SLR can change the current velocity and consequently, the sediment transport dynamics. Energy extraction can also reduce the overall magnitude of bed level adjustments [69]. Sediments settle in zones of low current velocities or where there is a sharp increase in the cross-sectional flow area. Thus, SLR can adjust the bed form through modifications of the current velocity and distribution of sediments. Further, in estuaries with strong relief, the depth often naturally and exponentially reduces from the mouth to the head [48]. To highlight the significance of different bed forms, Fig. 8 shows typical results on how the tidal stream power of mesotidal estuaries may be altered under SLR when Z = 80 km, Q/TP = 10%, n = 0.015 s/m$^{1/3}$, and θ = 0° and 0.004° (for details, see Section 2.1). It is observable that in cases with sloped beds (Fig. 8(b, d, f)) higher stream power is available in comparison to cases with flat beds (Fig. 8(a, c, e)) due to decreasing cross-sectional area and increasing current velocity. Further, a tilted bed can

modify the patterns of stream power in estuaries. To illustrate, a prismatic estuary has its maximum stream power at the mouth when a flat bed is considered (Fig. 8(a)), whereas the location of maximum stream power moves towards the head when a sloped bed is assumed (Fig. 8(b)). For this prismatic estuary, the stream power is dampened all the way from the entrance to the head in the case of a flat bed. The converse is valid if a sloped bed is considered. Therefore, variations in bed form, as an estuarine geomorphic alteration, can play an important role in determining the distribution of stream power and hotspots for tidal energy infrastructures.

In summary, changes in estuarine geomorphology (e.g., shape or bed form) may lead to a change in stream power distribution and hotspots. This geomorphic variation is an important aspect that has been largely absent in previous analytical, semi-analytical, and idealised studies.

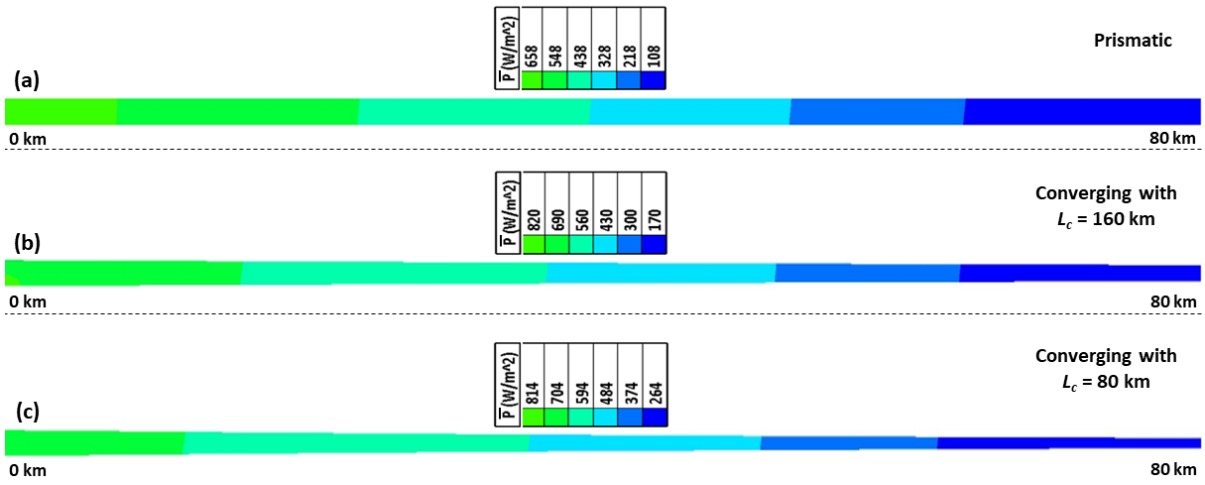

Fig. 7. Distribution of the averaged tidal stream power over a full spring-neap tidal cycle in (a) prismatic, (b) converging with L_c = 160 km, and (c) converging with L_c = 80 km macrotidal estuaries (TR_0 = 4 m) where Z = 80 km, Q/TP = 5% (medium river discharge), n = 0.03 s/m$^{1/3}$, θ = 0°, and SLR = 0 m.

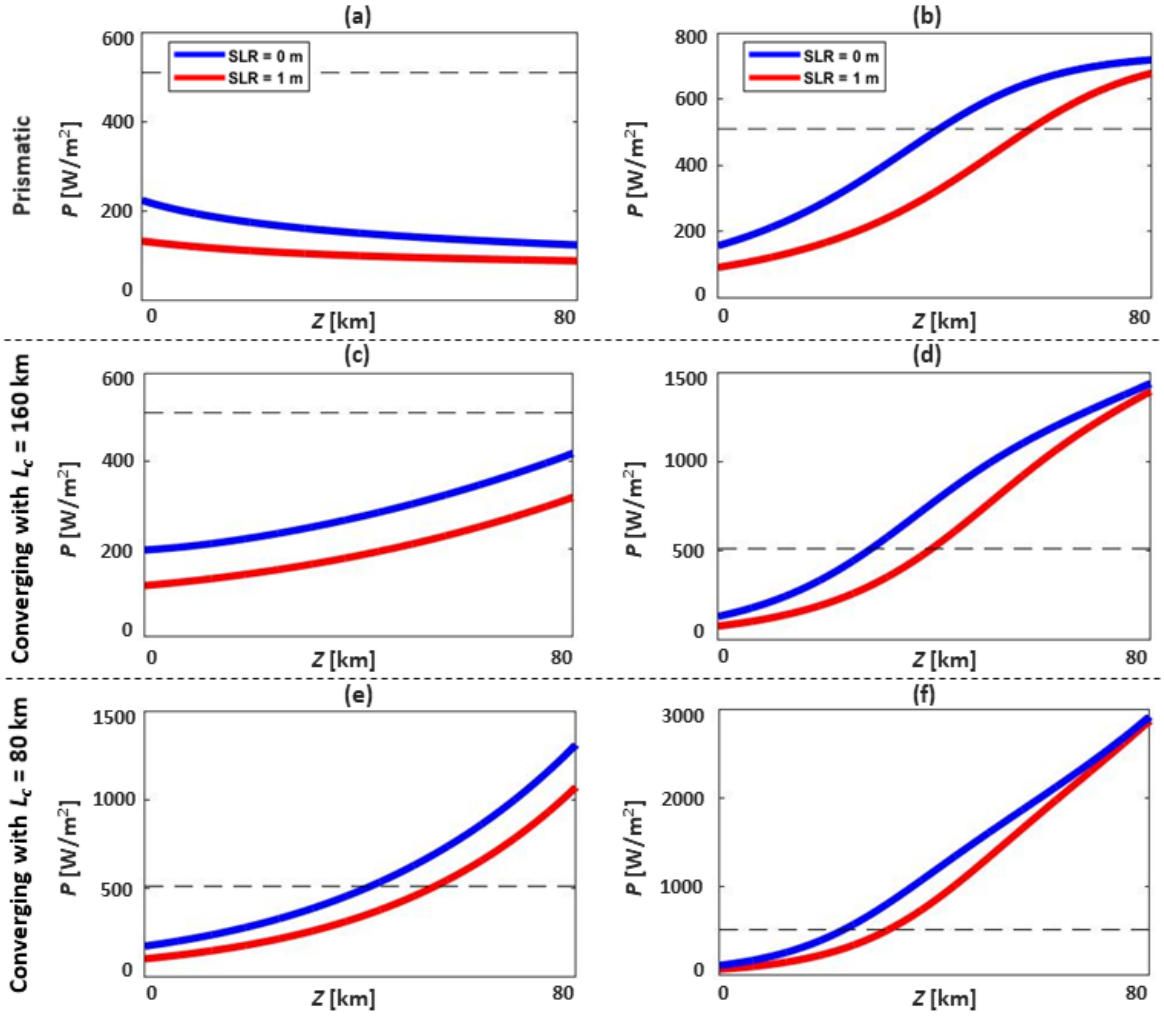

Fig. 8. Influence of bed slope on tidal stream power in (a, b) prismatic, (c, d) converging with L_c = 160 km, and (e, f) converging with L_c = 80 km mesotidal estuaries (TR_0 = 1 m) where Z = 80 km, Q/TP = 10%, n = 0.015 s/m$^{1/3}$, and θ = 0° (a, c, e) and 0.004° (b, d, f). Dashed lines show the applied feasibility thresholds for $V \geq 1$ m/s and $P \geq 510$ W/m^2.

4.2 Varying river inflow and tidal stream power

River inflow acts as an additional source of energy and interacts with the tidal energy, particularly in upstream areas [70]. As such, inflows contribute towards determining the strength and direction of flood and ebb tide currents [71], and hence, the location of sites to harness tidal energy [45]. A strong river inflow can also affect the distribution of sediments and thereby the overall shape of the estuarine system. For example, the shape of the Yangtze estuary varies from converging to prismatic depending upon the river discharge conditions

[72]. Fig. 9 indicates the influence of varying river inflows (Q/TP = 0, 1, 5, and 10%) on the stream power of mesotidal estuaries when Z = 40 km and n = 0.015 s/m$^{1/3}$. As is clear from this figure, varying river inflows (and their interaction with SLR) can significantly modify the patterns and values of stream power. For instance, in a converging estuary with L_c = 160 km, the power decreases from the mouth to the head when Q/TP = 0 and 1% (Fig. 9(e, f)), but increases when Q/TP = 5 and 10% (Fig. 9(g, h)). For a converging estuary with L_c = 80 km, the first few kilometres present more stream power when Q/TP = 0 and 1% (Fig. 9(i, j)), but change to the last few kilometres when Q/TP = 5 and 10% (Fig. 9(k, l)) as the energy of the river inflow overcomes frictional effects. Further, increasing river inflows would increase the stream power in all estuary types considered in this study. In this sense, it may be more appropriate to speak not of tidal stream energy but of hydrokinetic energy – kinetic energy of the flow produced by any combination of forcing mechanisms, not only by the tide. It goes without saying that the alterations in geomorphology and stream power under various river discharge conditions can pose a challenge for the performance of tidal stream turbines and electricity generation, requiring further attention.

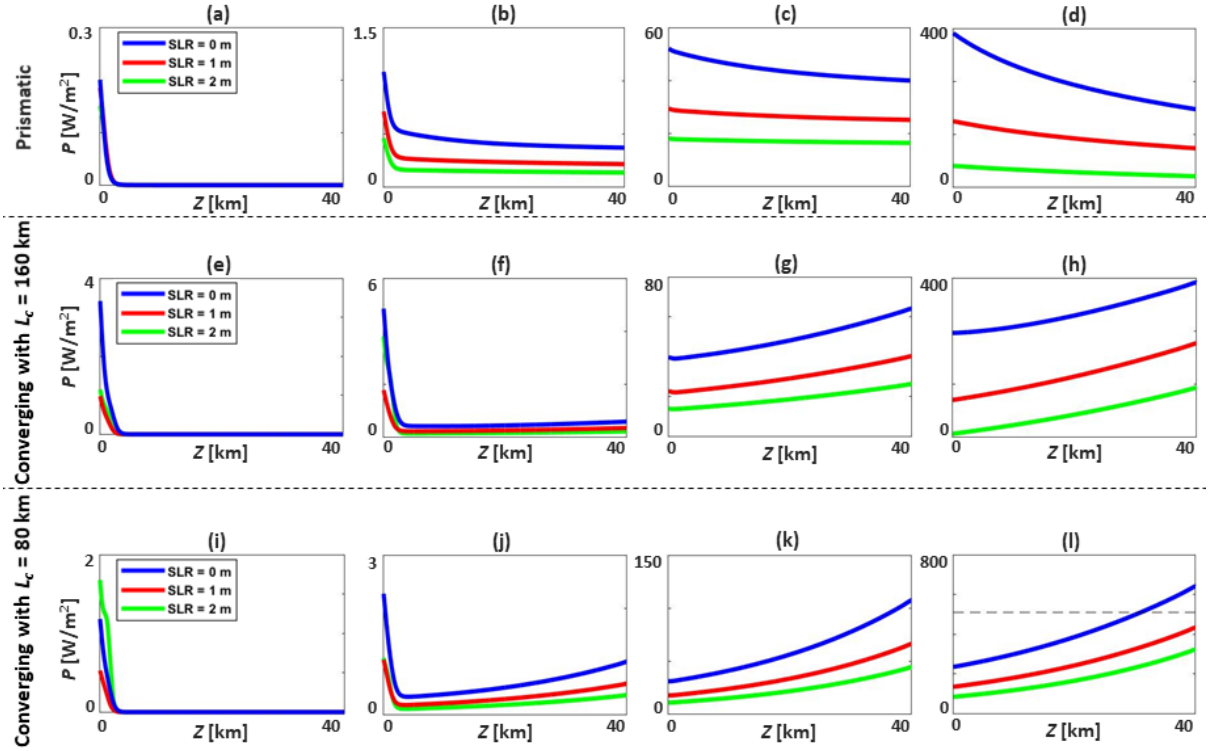

Fig. 9. Influence of varying river inflows on tidal stream power in (a-d) prismatic, (e-h) converging with L_c = 160 km, and (i-l) converging with L_c = 80 km mesotidal estuaries (TR_0 = 1 m) where Z = 40 km, Q/TP = 0% (a, e, i), 1% (b, f, j), 5% (c, g, k), and 10% (d, h, l), n = 0.015 s/m$^{1/3}$, and θ = 0°. Dashed line shows the applied feasibility threshold for $P \geq 510$ W/m^2.

5 Conclusions

Tidal stream energy is poised to play an important role in fulfilling the escalating energy demand of hundreds of millions of people who reside near estuaries worldwide. While SLR poses a challenge for future management and the development of tidal energy generation in estuarine environments, the majority of previous studies have disregarded its impacts on the tidal stream energy (power) of estuaries. To bridge this knowledge gap, a systematic study, comprising 978 estuarine hydrodynamic simulation cases, was conducted to provide insights into the changes that will be caused by SLR and river inflows to the tidal stream velocity, power, and the location of hotspots within different estuary types.

The results indicate that SLR can alter the spatial distribution of tidal stream power in various estuary types. Among the estuaries considered, cases with a high river inflow condition (due to large hydrokinetic energy) and/or a stronger converging shape (due to energy convergence) generally retain the largest tidal stream power. Prismatic estuaries exhibit less potential for tidal energy developments and experience the most drastic changes in tidal stream power in response to SLR, primarily to the downside. Estuaries with a stronger convergence length are likely to be the least influenced and the most promising systems for exploitation of tidal stream energy in present-day and future conditions. Further, SLR may eliminate or displace some hotspots that are currently practicable for harnessing tidal stream energy. Finally, estuary types likely to experience a reduced potential for tidal stream energy harvesting under certain values of SLR were identified. These changes to the existing tidal energy resource and the hotspot location have implications for development of tidal energy infrastructures, which should be taken into account by decision-makers. Given that the real time geomorphic adjustments were not considered in this study, if a real-world estuary matches one of the idealised cases tested in this work with potential for exploiting tidal stream energy, a detailed hydrodynamic modelling of the site would be recommended to accurately predict the tidal energy potential and location of hotspots, and how they may be affected by SLR. The findings of this present study may help managers identify suitable estuaries with the potential for tidal energy harvesting in present-day and future conditions, and therefore, in designing sustainable plans for the development of tidal energy, even in the absence of high-quality field data.

Acknowledgments

The authors would like to thank the editor and two anonymous reviewers for their insightful comments that improved this paper. The authors also thank Professor Ian King and Dr Valentin Heimhuber for helpful discussions regarding RMA-2 functions and estuarine tidal dynamics. Danial Khojasteh is supported by a UNSW Scientia PhD Scholarship.

References

[1] D. Khojasteh, D. Khojasteh, R. Kamali, A. Beyene, G. Iglesias. Assessment of renewable energy resources in Iran; with a focus on wave and tidal energy. Renewable and Sustainable Energy Reviews. 81 (2018) 2992-3005.

[2] M. Mestres, M. Griñó, J.P. Sierra, C. Mösso. Analysis of the optimal deployment location for tidal energy converters in the mesotidal Ria de Vigo (NW Spain). Energy. 115 (2016) 1179-87.

[3] V. Ramos, R. Carballo, M. Sanchez, M. Veigas, G. Iglesias. Tidal stream energy impacts on estuarine circulation. Energy Conversion and Management. 80 (2014) 137-49.

[4] A. Vazquez, G. Iglesias. Capital costs in tidal stream energy projects–A spatial approach. Energy. 107 (2016) 215-26.

[5] T.A. Adcock, S. Draper, R.H. Willden, C.R. Vogel. The Fluid Mechanics of Tidal Stream Energy Conversion. Annual Review of Fluid Mechanics. 53 (2021).

[6] D. Khojasteh, S.M. Mousavi, W. Glamore, G. Iglesias. Wave energy status in Asia. Ocean Engineering. 169 (2018) 344-58.

[7] J. Lelieveld, K. Klingmüller, A. Pozzer, R. Burnett, A. Haines, V. Ramanathan. Effects of fossil fuel and total anthropogenic emission removal on public health and climate. Proceedings of the National Academy of Sciences. 116 (2019) 7192-7.

[8] N. Guillou, S.P. Neill, P.E. Robins. Characterising the tidal stream power resource around France using a high-resolution harmonic database. Renewable Energy. 123 (2018) 706-18.

[9] D. Khojasteh, R. Kamali. Evaluation of wave energy absorption by heaving point absorbers at various hot spots in Iran seas. Energy. 109 (2016) 629-40.

[10] S. Radfar, R. Panahi, T. Javaherchi, S. Filom, A.R. Mazyaki. A comprehensive insight into tidal stream energy farms in Iran. Renewable and Sustainable Energy Reviews. 79 (2017) 323-38.

[11] J. Xia, R.A. Falconer, B. Lin. Numerical model assessment of tidal stream energy resources in the Severn Estuary, UK. Proceedings of the Institution of Mechanical Engineers, Part A: Journal of Power and Energy. 224 (2010) 969-83.

[12] M. Garcia-Oliva, S. Djordjević, G.R. Tabor. The influence of channel geometry on tidal energy extraction in estuaries. Renewable Energy. 101 (2017) 514-25.

[13] H. Díaz, J. Rodrigues, C.G. Soares. Preliminary assessment of a tidal test site on the Minho estuary. Renewable Energy. 158 (2020) 642-55.

[14] P.E. Robins, S.P. Neill, M.J. Lewis, S.L. Ward. Characterising the spatial and temporal variability of the tidal-stream energy resource over the northwest European shelf seas. Applied Energy. 147 (2015) 510-22.

[15] M. Sanchez, R. Carballo, V. Ramos, G. Iglesias. Energy production from tidal currents in an estuary: A comparative study of floating and bottom-fixed turbines. Energy. 77 (2014) 802-11.

[16] S.P. Neill, M.R. Hashemi. Fundamentals of ocean renewable energy: generating electricity from the sea. Academic Press, London, 2018.

[17] M. Nachtane, M. Tarfaoui, I. Goda, M. Rouway. A review on the technologies, design considerations and numerical models of tidal current turbines. Renewable Energy. 157 (2020) 1274-88.

[18] M. Grabbe, E. Lalander, S. Lundin, M. Leijon. A review of the tidal current energy resource in Norway. Renewable and Sustainable Energy Reviews. 13 (2009) 1898-909.

[19] V. Ramos, R. Carballo, M. Álvarez, M. Sánchez, G. Iglesias. A port towards energy self-sufficiency using tidal stream power. Energy. 71 (2014) 432-44.

[20] M. Mestres, P. Cerralbo, M. Grifoll, J.P. Sierra, M. Espino. Modelling assessment of the tidal stream resource in the Ria of Ferrol (NW Spain) using a year-long simulation. Renewable energy. 131 (2019) 811-7.

[21] D. Khojasteh, S. Hottinger, S. Felder, G. De Cesare, V. Heimhuber, D.J. Hanslow, et al. Estuarine tidal response to sea level rise: The significance of entrance restriction. Estuarine, Coastal and Shelf Science. 244 (2020) 106941.

[22] M. Marta-Almeida, M. Cirano, C.G. Soares, G.C. Lessa. A numerical tidal stream energy assessment study for Baía de Todos os Santos, Brazil. Renewable Energy. 107 (2017) 271-87.

[23] N. Yates, I. Walkington, R. Burrows, J. Wolf. Appraising the extractable tidal energy resource of the UK's western coastal waters. Philosophical Transactions of the Royal Society A: Mathematical, Physical and Engineering Sciences. 371 (2013) 20120181.

[24] T. El-Geziry, I. Bryden, S. Couch. Environmental impact assessment for tidal energy schemes: an exemplar case study of the Strait of Messina. Journal of Marine Engineering & Technology. 8 (2009) 39-48.

[25] I.D. Haigh, M.D. Pickering, J.M. Green, B.K. Arbic, A. Arns, S. Dangendorf, et al. The Tides They Are A-Changin': A Comprehensive Review of Past and Future Nonastronomical Changes in Tides, Their Driving Mechanisms, and Future Implications. Reviews of Geophysics. 58 (2020) e2018RG000636.

[26] S.A. Talke, D.A. Jay. Changing tides: The role of natural and anthropogenic factors. Annual Review of Marine Science. 12 (2020) 121-51.

[27] D. Rayner, W. Glamore, L. Grandquist, J. Ruprecht, K. Waddington, D. Khojasteh. Intertidal wetland vegetation dynamics under rising sea levels. Science of The Total Environment. 766 (2021) 144237.

[28] V. Masson-Delmotte, P. Zhai, A. Priani, S.L. Connors, C. Pean, S. Berger, et al. IPCC: Climate Change 2021: The Physical Science Basis. Contribution of Working Group I to the Sixth Assessment Report of the Intergovernmental Panel on Climate Change. Cambridge University Press. 2021.

[29] B.P. Horton, N.S. Khan, N. Cahill, J.S. Lee, T.A. Shaw, A.J. Garner, et al. Estimating global mean sea-level rise and its uncertainties by 2100 and 2300 from an expert survey. npj Climate and Atmospheric Science. 3 (2020) 1-8.

[30] T.E. Wong, A.M. Bakker, K. Keller. Impacts of Antarctic fast dynamics on sea-level projections and coastal flood defense. Climatic Change. 144 (2017) 347-64.

[31] J.L. Bamber, M. Oppenheimer, R.E. Kopp, W.P. Aspinall, R.M. Cooke. Ice sheet contributions to future sea-level rise from structured expert judgment. Proceedings of the National Academy of Sciences. 116 (2019) 11195-200.

[32] J. Du, J. Shen, Y.J. Zhang, F. Ye, Z. Liu, Z. Wang, et al. Tidal response to sea-level rise in different types of estuaries: The Importance of Length, Bathymetry, and Geometry. Geophysical Research Letters. 45 (2018) 227-35.

[33] K. Palmer, C. Watson, A. Fischer. Non-linear interactions between sea-level rise, tides, and geomorphic change in the Tamar Estuary, Australia. Estuarine, Coastal and Shelf Science. 225 (2019) 106247.

[34] B. Hong, J. Shen. Responses of estuarine salinity and transport processes to potential future sea-level rise in the Chesapeake Bay. Estuarine, Coastal and Shelf Science. 104 (2012) 33-45.

[35] T. Mulamba, P. Bacopoulos, E.J. Kubatko, G.F. Pinto. Sea-level rise impacts on longitudinal salinity for a low-gradient estuarine system. Climatic Change. 152 (2019) 533-50.

[36] J. Raw, T. Riddin, J. Wasserman, T. Lehman, T. Bornman, J. Adams. Salt marsh elevation and responses to future sea-level rise in the Knysna Estuary, South Africa. African Journal of Aquatic Science. 45 (2020) 49-64.

[37] K. Rogers, L.A. Mogensen, P. Davies, J. Kelleway, N. Saintilan, G. Withycombe. Impacts and adaptation options for estuarine vegetation in a large city. Landscape and Urban Planning. 182 (2019) 1-11.

[38] M. Sadat-Noori, C. Rankin, D. Rayner, V. Heimhuber, T. Gaston, C. Drummond, et al. Coastal wetlands can be saved from sea level rise by recreating past tidal regimes. Scientific reports. 11 (2021) 1-10.

[39] D. Khojasteh, W. Glamore, V. Heimhuber, S. Felder. Sea level rise impacts on estuarine dynamics: A review. Science of The Total Environment. (2021) 146470.

[40] J.M. González-Caballín, E. Álvarez, A.J. Guttiérrez-Trashorras, A. Navarro-Manso, J. Fernández, E. Blanco. Tidal current energy potential assessment by a two dimensional computational fluid dynamics model: The case of Avilés port (Spain). Energy Conversion and Management. 119 (2016) 239-45.

[41] F. O'Rourke, F. Boyle, A. Reynolds. Ireland's tidal energy resource; An assessment of a site in the Bulls Mouth and the Shannon Estuary using measured data. Energy Conversion and Management. 87 (2014) 726-34.

[42] H.S. Tang, S. Kraatz, K. Qu, G.Q. Chen, N. Aboobaker, C.B. Jiang. High-resolution survey of tidal energy towards power generation and influence of sea-level-rise: A case study at coast of New Jersey, USA. Renewable and Sustainable Energy Reviews. 32 (2014) 960-82.

[43] H.S. Tang, K. Qu, G.Q. Chen, S. Kraatz, N. Aboobaker, C.B. Jiang. Potential sites for tidal power generation: A thorough search at coast of New Jersey, USA. Renewable and Sustainable Energy Reviews. 39 (2014) 412-25.

[44] A. Mohammadian, B. Morse, J.-L. Robert. Assessment of tidal stream energy resources in a hypertidal estuary with highly irregular bathymetry using 3D numerical modelling. Journal of Ocean Engineering and Marine Energy. 5 (2019) 267-81.

[45] S.P. Neill, M.R. Hashemi, M.J. Lewis. The role of tidal asymmetry in characterizing the tidal energy resource of Orkney. Renewable Energy. 68 (2014) 337-50.

[46] J. Dronkers. Dynamics of coastal systems. World Scientific2005.

[47] D. Prandle. Estuaries: dynamics, mixing, sedimentation and morphology. Cambridge University Press2009.

[48] H.H. Savenije. Salinity and tides in alluvial estuaries. Gulf Professional Publishing2005.

[49] L.C. van Rijn. Analytical and numerical analysis of tides and salinities in estuaries; part I: tidal wave propagation in convergent estuaries. Ocean Dynamics. 61 (2011) 1719-41.

[50] D.L. Passeri, S.C. Hagen, S.C. Medeiros, M.V. Bilskie, K. Alizad, D. Wang. The dynamic effects of sea level rise on low-gradient coastal landscapes: A review. Earth's Future. 3 (2015) 159-81.

[51] G.J. Arcement, V.R. Schneider. Guide for selecting Manning's roughness coefficients for natural channels and flood plains. US Government Printing Office Washington, DC1989.

[52] J.R. Leuven, H.J. Pierik, M. van der Vegt, T.J. Bouma, M.G. Kleinhans. Sea-level-rise-induced threats depend on the size of tide-influenced estuaries worldwide. Nature Climate Change. 9 (2019) 986-92.

[53] R.I. Ferguson. River channel slope, flow resistance, and gravel entrainment thresholds. Water Resources Research. 48 (2012).

[54] H. Cai, M. Toffolon, H.H. Savenije, Q. Yang, E. Garel. Frictional interactions between tidal constituents in tide-dominated estuaries. Ocean Science. 14 (2018) 769-82.

[55] R. Carballo, G. Iglesias, A. Castro. Numerical model evaluation of tidal stream energy resources in the Ría de Muros (NW Spain). Renewable Energy. 34 (2009) 1517-24.

[56] W.-B. Chen, W.-C. Liu. Assessing the influence of sea level rise on tidal power output and tidal energy dissipation near a channel. Renewable Energy. 101 (2017) 603-16.

[57] I. King, B. Donnell, J. Letter, W. McANALLY, W. Thomas. Users Guide to RMA2 WES Version 4.5. The US Army Corps of Engineers–Waterways experiment laboratory. (1997) 240.

[58] D. Khojasteh, W. Glamore, V. Heimhuber, S. Hottinger, S. Felder. Implications of tidal resonance and water depth on predicting sea level rise in estuaries. Australasian Coasts and Ports. Engineers Australia, Hobart, Australia, 2019. p. 707.

[59] I. King. A Two-dimensional Finite Element Model for Flow in Estuaries and Streams. RMA-2, Users Guide, Version 84 T. (2013).

[60] M. Lewis, S.P. Neill, P.E. Robins, M.R. Hashemi. Resource assessment for future generations of tidal-stream energy arrays. Energy. 83 (2015) 403-15.

[61] D. Khojasteh, S. Chen, S. Felder, V. Heimhuber, W. Glamore. Estuarine tidal range dynamics under rising sea levels. PloS one. 16 (2021) e0257538.

[62] I. Robinson. Tides in the Bristol Channel—an analytical wedge model with friction. Geophysical Journal International. 62 (1980) 77-95.

[63] R.W. Dalrymple, K. Choi. Morphologic and facies trends through the fluvial–marine transition in tide-dominated depositional systems: A schematic framework for environmental and sequence-stratigraphic interpretation. Earth-Science Reviews. 81 (2007) 135-74.

[64] K. Dyer. Estuaries: A Physical Introduction (2nd Edition): John Wiley and Sons1997.

[65] C.T. Friedrichs, D.G. Aubrey. Tidal propagation in strongly convergent channels. Journal of Geophysical Research: Oceans. 99 (1994) 3321-36.

[66] D.K. Ralston, S. Talke, W.R. Geyer, H.A.M. Al-Zubaidi, C.K. Sommerfield. Bigger Tides, Less Flooding: Effects of Dredging on Barotropic Dynamics in a Highly Modified Estuary. Journal of Geophysical Research: Oceans. 124 (2019) 196-211.

[67] H. De Swart, J. Zimmerman. Morphodynamics of tidal inlet systems. Annual review of fluid mechanics. 41 (2009) 203-29.

[68] A.R. Carrasco, T. Plomaritis, J. Reyns, Ó. Ferreira, D. Roelvink. Tide circulation patterns in a coastal lagoon under sea-level rise. Ocean Dynamics. 68 (2018) 1121-39.

[69] S.P. Neill, E.J. Litt, S.J. Couch, A.G. Davies. The impact of tidal stream turbines on large-scale sediment dynamics. Renewable Energy. 34 (2009) 2803-12.

[70] T. Kukulka, D.A. Jay. Impacts of Columbia River discharge on salmonid habitat: 1. A nonstationary fluvial tide model. Journal of Geophysical Research: Oceans. 108 (2003).

[71] R. Uncles, J. Stephens, C. Harris. Towards predicting the influence of freshwater abstractions on the hydrodynamics and sediment transport of a small, strongly tidal estuary: The Devonshire Avon. Ocean & coastal management. 79 (2013) 83-96.

[72] M. Zhang, I. Townend, Y. Zhou, H. Cai. Seasonal variation of river and tide energy in the Yangtze estuary, China. Earth Surface Processes and Landforms. 41 (2016) 98-116.